Eur. Phys. J. D **18**, 261–266 (2002)
DOI: 10.1140/epjd/e20020046

THE EUROPEAN PHYSICAL JOURNAL D
EDP Sciences

Quenching of metastable antiprotonic helium atoms in collisions with deuterium molecules

B. Juhász[1,a], J. Eades[2], R.S. Hayano[3], M. Hori[2], D. Horváth[4], T. Ishikawa[3], J. Sakaguchi[3], H.A. Torii[5], E. Widmann[3], H. Yamaguchi[3], and T. Yamazaki[6]

[1] Institute of Nuclear Research of the Hungarian Academy of Sciences, 4001 Debrecen, Hungary
[2] CERN, 1211 Geneva 23, Switzerland
[3] Department of Physics, University of Tokyo, 7-3-1 Hongo, Bunkyo-ku, Tokyo 113, Japan
[4] KFKI Research Institute for Particle and Nuclear Physics, 1525 Budapest, Hungary
[5] Institute of Physics, University of Tokyo, 3-8-1 Komaba, Meguro-ku, Tokyo 153, Japan
[6] RI Beam Science Laboratory, RIKEN, Wako, Saitama 351-0198, Japan

Received 6 July 2001

Abstract. Quenching of metastable antiprotonic helium atoms in collisions with deuterium molecules has been studied using laser spectroscopy at CERN's new Antiproton Decelerator facility. The quenching cross-sections of the states $(n, l) = (39, 36)$, $(39, 37)$, and $(39, 38)$ were determined from the decay rates of the states which were observed using the "deuterium-assisted inverse resonance" (DAIR) method. The results revealed a similar (n, l)-dependence of the quenching cross-sections as in the case of hydrogen but the values were smaller by a factor of ∼1.5.

PACS. 36.10.-k Exotic atoms and molecules (containing mesons, muons, and other unusual particles) – 42.62.Fi Laser spectroscopy – 34.20.Gj Intermolecular and atom-molecule potentials and forces

1 Introduction

About 3% of antiprotons stopped in helium are known to survive with an average lifetime of a few microseconds [1–6]; no such anomalously long lifetime has been found, however, in other materials [1,3,4]. This phenomenon has been attributed to formation of metastable $\overline{\mathrm{p}}\mathrm{He}^+ \equiv \overline{\mathrm{p}} - \mathrm{e}^- - \mathrm{He}^{2+}$ states [7,8]. The long lifetime of this $\overline{\mathrm{p}}\mathrm{He}^+$ system is nearly independent of the density of the helium gas target and can be observed even in liquid and solid helium [4]. Admixtures of various foreign gases, on the other hand, have quite drastic effects [2,3,6,9]. A laser resonance method has been developed and applied to transitions between pairs of "metastable" and "short-lived" states [10–14]. This has provided rich information on the transition energies and the lifetimes and populations of the relevant states. The quenching cross-sections of metastable states in collisions with hydrogen molecules have been measured using this laser tagging method [15]. These experiments revealed that higher-lying (larger-n) metastable states are quenched more strongly than lower-lying ones. Consequently, adding a suitably chosen quantity of hydrogen to the helium gas can turn a normally long-lived state (n, l) into a short-lived one, while retaining the longevity of an adjacent lower-lying state (n', l'). It is then possible to induce a laser transition from the lower-lying state to the upper-lying one ("inverse resonance"). This technique, which we call hydrogen-assisted inverse resonance (HAIR) method [16], has allowed us to measure the quenching cross-sections of six more antiprotonic states [17]; the results showed a systematic dependence of the quenching cross-sections on (n, l): metastable states with larger n are quenched more strongly and metastable states with the same n but larger l are quenched less strongly than those with smaller l. Later quenching cross-sections with deuterium have also been obtained using "ordinary" transitions *i.e.* transitions from metastable to naturally short-lived states [18].

Some theoretical models of the $\overline{\mathrm{p}}\mathrm{He}^+ - \mathrm{H}_2$ interaction potential have suggested the existence of a potential barrier [19,20] which increases with decreasing n, in qualitative agreement with the experimental tendency. However, no quantitative calculations for the quenching cross-sections have yet been done. It was therefore very important to provide further experimental information, in particular, on the $\mathrm{H}_2/\mathrm{D}_2$ isotope effect since this could give important keys for understanding the $\mathrm{H}_2/\mathrm{D}_2$ quenching phenomena more deeply. In this paper we describe the measurement of the quenching cross-section of three states of $\overline{\mathrm{p}}\mathrm{He}^+$, $(n, l) = (39, 36)$, $(39, 37)$, and $(39, 38)$, employing the deuterium counterpart of the HAIR method (DAIR).

[a] e-mail: bertalan.juhasz@cern.ch

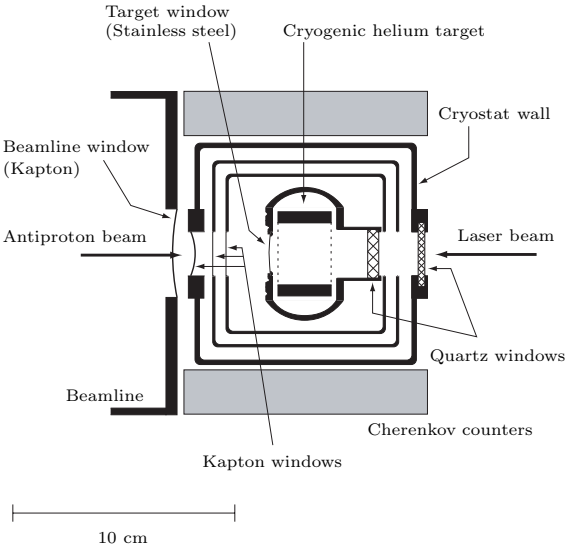

Fig. 1. Top view of our experimental setup. The inner rectangular part with dashed vertical lines is a microwave cavity which was not used during the current experiment.

2 Experimental details

2.1 Antiproton source

The experiments were performed at CERN's new Antiproton Decelerator facility (AD) [21] which provided a pulsed beam with an energy of 5.3 MeV (momentum: 100 MeV/c) and pulse length of ∼250 ns (Gaussian FWHM) at a repetition rate of 1 pulse per 144 seconds. Each pulse contained $\sim 2 \times 10^7$ antiprotons. Although this was approximately one order of magnitude less than in our previous experiments at LEAR (Low Energy Antiproton Ring), the pulse repetition rate was higher and the intensity was more stable. The X–Y distribution and the intensity of each incoming $\overline{\mathrm{p}}$ pulse were measured by a parallel plate secondary emission chamber placed just upstream of the AD beam line window.

2.2 Annihilation detection

Samples of antiprotonic helium atoms were readily produced by stopping AD antiproton pulses in a cryogenic helium gas target (see Fig. 1). The stopping distribution of the antiprotons was optimized with the help of Monte Carlo simulations [3,22]. The annihilation products (mainly charged pions) were detected by two Cherenkov counters which were made of UV-transparent Lucite plates with a thickness of 2 cm. They covered a solid angle of $\sim 2\pi$ sr around the target providing a detection efficiency greater than 85% for $\overline{\mathrm{p}}$ annihilations. The Cherenkov light pulse coming from the counters was collected by two gatable fine-mesh photomultipliers (Hamamatsu Photonics R5505GX-ASSYII) developed for our experiments. About 97% of the antiprotons annihilate promptly in the target without forming metastable $\overline{\mathrm{p}}\mathrm{He}^+$ atoms, and the many simultaneous pions from these annihilations produce a high intensity pulse of Cherenkov light. To protect the photomultipliers against saturation, they were deactivated during the antiproton pulse arrival by adjusting the voltages on the dynodes. The outputs of the photomultipliers were recorded using a digital oscilloscope with an analog bandwidth of 1 GHz.

2.3 Helium target

Our gas target consisted of ^{4}He (purity: 99.9999%) to which deuterium (purity: 99.8%) was premixed at molar concentrations of 301 ppm and 1 000 ppm with a relative accuracy of 2%. To avoid contamination by impurity gases (*e.g.* nitrogen and oxygen) the gas target was kept at a constant temperature of 30 K during the measurements. The temperature was measured with a silicon diode sensor (LakeShore DT-470) mounted on the outer surface of the target chamber. A conservative systematic error of 2.0 K was assigned to the temperature values which included both the calibration error of the sensor and the temperature difference between the interior of the target chamber and the location of the sensor. The temperature variation during the experiment was only 0.01–0.1 K. The absolute number density of D_2 molecules was varied by changing the pressure of the gas target between 1 and 4 bar. Although increasing pressure decreases the lifetime of metastable states, this effect is negligible compared to the lifetime shortening caused by the increasing density of the D_2 molecules [23]. The pressure of the gas target was measured with a Baratron absolute capacitance manometer (MKS 121AA) with an accuracy of 5 mbar.

2.4 Laser system

As described in [10–14], laser beams can be tuned to resonate between two states of $\overline{\mathrm{p}}\mathrm{He}^+$, one of which is metastable and the other one is short-lived. For the present experiment a new laser setup was designed [24] in which a dye laser (Lambda Physik Scanmate 2E) pumped by the second harmonic of a Nd:YAG laser (Coherent Infinity) irradiated our cryogenic helium gas target after each antiproton pulse. The laser firing time was synchronized to the arrival of the antiproton pulse by a trigger signal from the AD. Each laser pulse had a width of 4–6 ns, a diameter of ∼1 cm, a bandwidth of ∼3 GHz, and a power density of ~ 1.0 mJ/cm^2. The laser shot-to-shot intensity fluctuation was ∼ 4%. The spatial and time profile, and intensity of each laser pulse at the target position were recorded with a CCD camera, a UV-sensitive, high bandwidth (f = 1 GHz) p-i-n photodiode and a pyroelectric detector, respectively.

3 Shape of the annihilation time spectra

3.1 Without laser irradiation

The time spectrum of the annihilation of antiprotons contained in a single AD shot is a superposition of (i) the

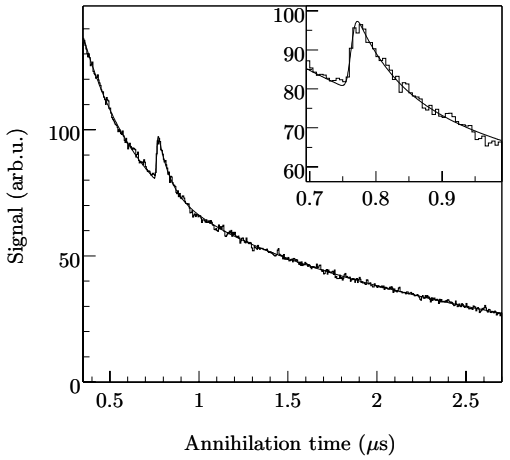

Fig. 2. A summed-up analog delayed annihilation time spectrum of the transition $(n, l) = (38, 36) \rightarrow (39, 37)$ measured at 30 K, 3.93 bar and deuterium concentration of 301 ppm. This spectrum was obtained by adding 15 time spectra together. The inset shows an enlarged view of the laser-induced annihilation peak. The solid lines represent the result of fitting the sum of equations (1, 2) to the spectrum. The annihilation time is measured from the mean arrival time of the antiproton pulse.

sharp (∼250 ns long) prompt annihilation peak described in Section 2.2, (ii) the 3% delayed annihilation signal under study, with a duration of about 15 μs, and (iii) an exponentially decaying component with a decay constant of 2.2 μs (μ^+ lifetime), arising from those pions in the prompt peak annihilations which stop in the material surrounding the helium target and subsequently decay *via* the $\pi^+ \rightarrow \mu^+ \rightarrow e^+$ chain. Since the two photomultipliers were only reactivated after the initial prompt peak, their output, henceforth referred to as the analogue delayed annihilation time spectra, contain only (ii) and (iii). Thus a spectrum without laser irradiation, which we call the "background", can be described by the sum of a single exponential and a composite function which reflects the very complicated cascade process. It turned out, however, that the sum of two exponentials and a constant function can reproduce the background fairly well (see Fig. 2) provided that the fitting region is shorter than ∼5 μs. Thus the background function we used in the fit is

$$B(t) = N[\gamma_\mathrm{b} f \exp(-\gamma_\mathrm{b} t) + \gamma_\mu (1-f) \exp(-\gamma_\mu t)] + C, \quad (1)$$

where γ_μ is the decay rate of the $\pi^+ \rightarrow \mu^+ \rightarrow e^+$ decay chain and therefore fixed to $(2.2\ \mu\mathrm{s})^{-1}$ while γ_b is a free parameter, f is the fraction of the delayed annihilation events in the total spectrum, C is a time-independent constant, and N is a normalization factor; thus equation (1) contains 4 free parameters.

3.2 With laser irradiation

When a laser pulse with wavelength tuned to a "metastable to short-lived" transition wavelength is fired into the target containing $\overline{\mathrm{p}}\mathrm{He}^+$ atoms an additional peak appears in the annihilation time spectrum at the instant of the application of the laser pulse as seen in Figure 2. This is a result of the sudden increase in the population of the shorter-lived antiprotonic state. In the present experiment, the laser pulse was generated just a few hundred nanoseconds after reactivating the photomultipliers at which time the population of the long-lived state was still sufficient to produce a strong peak. After the laser irradiation the peak decays with the lifetime of the shorter-lived daughter state (which is the lower energy state in case of "ordinary" transitions and the upper one in case of HAIR and DAIR transitions). In fact, this exponential function is convoluted with an approximately Gaussian laser time profile broadened by the photomultiplier response time (∼5 ns). The effect of Rabi oscillations on the peak structure can be neglected in the present case [10]. As a result, the time evolution of the peak can be described by a function which is a product of an exponential and a complementary error function:

$$P(t) = \frac{1}{2} N \gamma_\mathrm{p} f f_\mathrm{p} \,\mathrm{erfc}\left(\frac{t_0 + \sigma^2 \gamma_\mathrm{p} - t}{\sigma\sqrt{2}}\right) \times \exp\left[-\gamma_\mathrm{p}\left(t - t_0 - \sigma^2\gamma_\mathrm{p}/2\right)\right]; \quad (2)$$

$$\mathrm{erfc}(x) = 1 - \mathrm{erf}(x) = 1 - \frac{2}{\sqrt{\pi}} \int_0^x \exp(-t^2)\mathrm{d}t.$$

Here γ_p is the peak decay rate, t_0 and σ are the centroid and width of the laser time profile, respectively, f_p is the fraction of the corresponding antiprotonic state in the total number of delayed annihilation events, while f and N are the same parameters as in equation (1).

4 Fitting procedures

4.1 Spectrum summing-up

For single AD shots of typical intensity the statistical significance of the resonance peak was too small to obtain reliable decay rate data. Therefore spectra from 15 AD shots (all measured under the same target conditions) were added together to get two summed-up time spectra for the two Cherenkov counters. In the present experiment the shot to shot fluctuation of laser timing was less than 1 ns, which justifies this addition of different ADATS from the same counter. As the two Cherenkov counters may have different characteristics, a spectrum of one of them cannot be simply added to that of the other. Thus the two summed-up time spectra were fitted simultaneously using the sum of equations (1, 2) with the same values for the parameters γ_b, γ_p, f_p, t_0, and σ, respectively, but with different values for N^i, f^i, and C^i $(i = 1, 2)$.

4.2 Error assignment

Since the data were sampled in an analog way it was essential to assign correct errors to each bin. Generally,

Table 1. Decay rates $\gamma(n,l)$ of three metastable antiprotonic states measured at a temperature T and a pressure p with a deuterium concentration of c_{D_2}; the corresponding number density of D_2 molecules n_{D_2} is also shown. The last column contains the theoretical decay rate of the given metastable state without collisional quenching [8,27]. The errors of the values contain both the statistical and systematical errors summed quadratically.

(n,l)	T (K)	p (mbar)	c_{D_2} (ppm)	n_{D_2} (10^{16} cm^{-3})	$\gamma(n,l)$ $(\mu s)^{-1}$	$\gamma_0(n,l)$ $(\mu s)^{-1}$
$(39,36)$	30.0 ± 2.0	993 ± 5	301 ± 6	7.2 ± 0.5	6.9 ± 0.3	
	30.0 ± 2.0	1956 ± 14	301 ± 6	14.2 ± 1.0	13.4 ± 1.2	
						0.62
$(39,37)$	30.0 ± 2.0	1931 ± 6	301 ± 6	14.0 ± 1.0	7.5 ± 0.2	
	30.0 ± 2.0	3926 ± 43	301 ± 6	28.5 ± 2.0	16.3 ± 0.5	
	30.0 ± 2.0	1998 ± 5	1000 ± 20	48.3 ± 3.4	27.7 ± 2.1	
						0.62
$(39,38)$	30.0 ± 2.0	3789 ± 7	301 ± 6	27.5 ± 1.9	4.6 ± 0.2	
	30.0 ± 2.0	2017 ± 11	1000 ± 20	48.7 ± 3.4	8.6 ± 0.2	
	30.0 ± 2.0	3810 ± 68	1000 ± 20	92.0 ± 6.6	18.9 ± 0.8	
						0.62

the error of the signal originates from (i) the fluctuations of the number of delayed annihilations and (ii) fluctuations of the amount of Cherenkov light of one detected annihilation. In our case, these fluctuations cannot be estimated with reliable accuracy, the bin errors were therefore determined from the fluctuations of the bin contents. We used the fact that if the bin errors are purely statistical then the distribution of the bin contents is Gaussian and the error of a bin is proportional to the square root of the bin content. The constant proportionality factor for a given spectrum was determined as follows: first, the summed-up time spectrum was rebinned from the original 0.5 ns to 5 ns bin width to eliminate a ∼100 MHz ringing from the photomultipliers. The signal from the oscilloscope may have a constant offset which needs to be subtracted from the spectrum. This offset was determined by fitting a constant function to a spectrum range where only this constant background was present. The spectrum range chosen was 1 μs long and started 15 μs after the antiprotonic atom formation. Afterwards, a single exponential function $f_e(t)$ was fitted to a narrow region (t_s, t_f) of the spectrum outside the peak. Finally, a histogram was constructed from the difference of the bin contents from $f_e(t)$ and a Gaussian function was fitted to this histogram. If the width of this Gaussian is σ_e, then the error σ_i of each bin i can be estimated as:

$$\sigma_i = \frac{\sigma_e}{\sqrt{V_c}} \sqrt{V_i}, \tag{3}$$

where V_i is the content in bin i, and V_c is the value of the fitted exponential in the center of the fitting region *i.e.* $V_c = f_e(t_c)$, $t_c = (t_s + t_f)/2$. Fitting the time spectra with these errors gave reasonable χ^2 values (χ^2/d.o.f. ≈ 0.8–1.2) in agreement with the visual goodness of the fits shown in Figure 2. Repeating the above method using different fitting regions with smaller and larger average bin contents we obtained similar bin errors which justifies our assumption that the bin errors were statistical.

4.3 Observed decay rates

Fitting the time spectra with the sum of equations (1, 2) using the above method, we determined the decay rates of the metastable states $(n,l) = (39,36)$ using the transition $(38,35) \rightarrow (39,36)$, $(39,37)$ using the transition $(38,36) \rightarrow (39,37)$, and $(39,38)$ using the transition $(38,37) \rightarrow (39,38)$. The corresponding laser wavelengths of $\lambda = 597.298$ nm, 597.397 nm, and 597.607 nm, respectively, were taken from [16]. The results and the target conditions are summarized in Table 1. Besides the data listed there we also tried to measure the decay rate of the state $(39,36)$ at 30 K, 4 bar, and deuterium concentration of 301 ppm but no peak was observable, suggesting that at such a high deuterium concentration the parent state $(38,35)$ is already completely quenched. This is a quite surprising result since during our previous measurements at LEAR, with target conditions of 30.2 K, 3.03 bar, and hydrogen concentration of 291 ppm the peak was clearly visible [16,17]. So far, no explanation has been found to this deviation.

5 Quenching cross-sections

From our previous measurements with hydrogen and deuterium we concluded that the decay rate of a given metastable antiprotonic state increases linearly with increasing density of H_2 and D_2 molecules [15,17,18]. This indicates that these metastable states are quenched in binary collisions with the foreign gas molecules. The decay rate of the state then can be expressed as

$$\gamma(n,l) = \gamma_0(n,l) + n_{D_2}\, v_{th}\, \sigma_q^{D_2}(n,l), \tag{4}$$

i.e. the sum of the decay rate $\gamma_0(n,l)$ in pure helium and the rate of quenching caused by collisions [15]. Here n_{D_2} is the number density of deuterium molecules, $v_{th} = \sqrt{8kT/(\pi M_{red})}$ is the relative velocity of the colliding molecules [25] (where k denotes the Boltzmann constant,

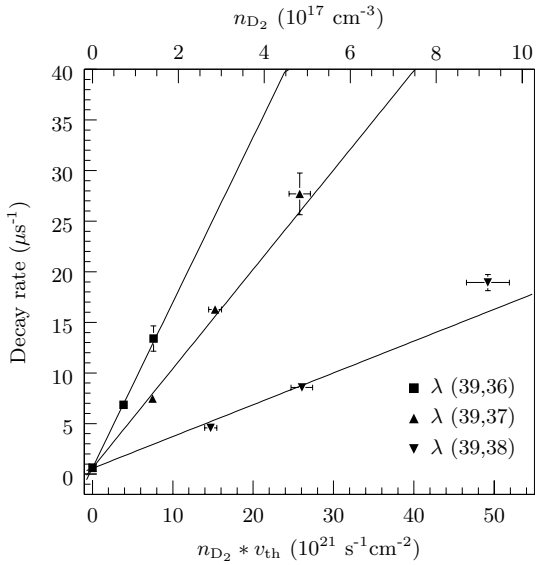

Fig. 3. Decay rates of three metastable antiprotonic states *versus* the flux $n_{D_2} \times v_{th}$. The top axis shows the approximate number density of D_2 molecules. The solid lines represent the results of fitting equation (4) to the experimental and theoretical decay rates.

Table 2. Quenching cross-sections $\sigma_q^{D_2}(n,l)$ obtained from fitting equation (4) to the experimental and theoretical decay rates listed in Table 1. The cross-sections $\sigma_q^{H_2}(n,l)$ from previous measurements [17] are also shown for comparison. The values are in units of 10^{-16} cm^2.

(n,l)	$\sigma_q^{D_2}(n,l)$	$\sigma_q^{H_2}(n,l)$
$(39,36)$	16.3 ± 1.0	25.8 ± 1.0
$(39,37)$	9.8 ± 0.4	13.4 ± 1.3
$(39,38)$	3.1 ± 0.3	5.4 ± 0.4

T the target gas temperature, and M_{red} the reduced mass of the $D_2 - \overline{p}He^+$ system), and $\sigma_q^{D_2}(n,l)$ is the state-dependent collisional quenching cross-section. The $\overline{p}He^+$ atoms are assumed to be thermalized before they collide with D_2 molecules since the thermalization time from a few eV (*i.e.* initial kinetic energy after $\overline{p}He^+$ formation) is much shorter than the typical lifetime of a metastable antiprotonic state [26].

Decay rates of the states $(39,36)$, $(39,37)$, and $(39,38)$ in pure helium cannot be measured since these states are not accessible with conventional laser spectroscopy. Therefore the calculated theoretical decay rates [7,8,27] were used as values for $\gamma_0(n,l)$ (see last column of Tab. 1). As in the previous measurements, an error of 15% was assigned to each of these values [17].

Figure 3 shows the measured decay rates of the three antiprotonic states *versus* the flux $n_{D_2} \times v_{th}$; the solid lines represent the results of fitting equation (4) to the experimental and theoretical decay rates. The quenching cross-sections obtained from the fits are listed in Table 2.

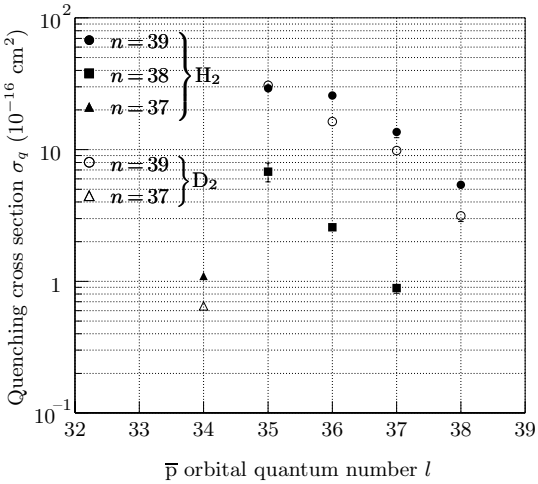

Fig. 4. The (n,l)-dependence of the quenching cross-section σ_q for both hydrogen and deuterium. The figure contains all the cross-sections which have been measured so far; the three new measurements are indicated with empty circles at $n = 39$ and $l = 36$, 37, and 38.

6 Conclusions

Figure 4 summarizes the quenching cross-sections which have been measured so far with hydrogen and deuterium. The new results (three points in the plot) clearly show that the (n,l)-dependence of quenching by deuterium is very similar to that by hydrogen; the cross-section values, however, are systematically smaller in the case of deuterium by a factor of $\sim$1.5. Only the state $(39,35)$ shows the same σ_q values for H_2 and D_2. This difference in the quenching cross-sections cannot be explained by the different thermal velocities of H_2 and D_2 molecules since the collisional velocities were already factored out when we deduced the cross-sections. The cross-section ratio of about 1.5, however, is suggestive of the inverse square root of the mass ratio, which is often encountered in tunneling phenomena of hydrogenic particles.

Sauge *et al.* used *ab initio* quantum chemistry methods to calculate the potential energy surface of the $\overline{p}He^+$ and H_2 molecule and found that an (n,l)-dependent activation barrier exists for reactive channels [19,20] which could qualitatively explain the (n,l)-dependence of the quenching cross-section. Their model can also explain why the cross-section of the state $(39,35)$ is not considerably higher than that of the state $(39,36)$: the activation barrier already vanishes for the state $(39,36)$ at 30 K which maximizes the quenching cross-section, therefore decreasing l cannot increase it any further.

More experimental data can be easily obtained by measuring the quenching cross-sections of the states with $n = 38$ and $l = 35$, 36, and 37 using DAIR transitions. The temperature dependence of quenching by H_2 and D_2 molecules can be investigated systematically at higher temperatures, which will reflect the (n,l)-dependent barrier heights in comparison with the collisional energy.

We are indebted to the AD and PS staff at CERN for their tireless dedication in providing us with the new machine and antiproton beam, and J.-M. Rieubland and his team for their help on many aspects of the helium target chamber and cryogenic system. We are grateful to Dr. P. Valiron and S. Sauge for providing us with their theoretical results. The present work was supported by the Grant-in-Aid for Creative Basic Research (10NP0101) of the Japanese Ministry of Education, Culture, Sports, Science, and Technology, and the Hungarian Scientific Research Fund (OTKA T033079 and TeT JAP-4/98). M.H. acknowledges the support of the Japan Society for the Promotion of Science.

References

1. M. Iwasaki *et al.*, Phys. Rev. Lett. **67**, 1246 (1991).
2. T. Yamazaki *et al.*, Nature **361**, 238 (1993).
3. S.N. Nakamura *et al.*, Phys. Rev. A **49**, 4457 (1994).
4. E. Widmann *et al.*, Phys. Rev. A **51**, 2870 (1995).
5. B. Ketzer *et al.*, Phys. Rev. A **53**, 2108 (1996).
6. E. Widmann *et al.*, Phys. Rev. A **53**, 3129 (1996).
7. T. Yamazaki, K. Ohtsuki, Phys. Rev. A **45**, 7782 (1992).
8. I. Shimamura, Phys. Rev. A **46**, 3776 (1992).
9. R. Pohl *et al.*, Phys. Rev. A **58**, 4406 (1998).
10. N. Morita, K. Ohtsuki, T. Yamazaki, Nucl. Instrum. Meth. A **330**, 439 (1993).
11. N. Morita *et al.*, Phys. Rev. Lett. **72**, 1180 (1994).
12. R.S. Hayano *et al.*, Phys. Rev. Lett. **73**, 1485 (1994); Errata **73**, 3181 (1994).
13. F.E. Maas *et al.*, Phys. Rev. A **52**, 4266 (1995).
14. T. Yamazaki *et al.*, Phys. Rev. A **55**, R3295 (1997).
15. T. Yamazaki *et al.*, Chem. Phys. Lett. **265**, 137 (1997).
16. B. Ketzer *et al.*, Phys. Rev. Lett. **78**, 1671 (1997).
17. B. Ketzer *et al.*, J. Chem. Phys. **109**, 424 (1998).
18. B. Ketzer *et al.*, Eur. Phys. J. D **13**, 305 (2001).
19. S. Sauge, P. Valiron, J. Carbonell, Few Body Sys. Suppl. **10**, 211 (1999).
20. S. Sauge, P. Valiron, Chem. Phys. (submitted).
21. S. Maury, CERN/PS 99-50 (HP) (unpublished).
22. B. Juhász, M.Sc. thesis, University of Debrecen, 2000.
23. M. Hori *et al.*, Phys. Rev. A **58**, 1612 (1998).
24. M. Hori *et al.*, Phys. Rev. Lett. **87**, 093401 (2001).
25. J.B. Hasted, *Physics of atomic collisions*, 2nd edn. (Butterworth & Co., London, 1972).
26. F.J. Hartmann *et al.*, Phys. Rev. A **58**, 3604 (1998).
27. V.I. Korobov, I. Shimamura, Phys. Rev. A **56**, 4587 (1997).